

Article

Investigation into Biomass Tar-Based Carbon Deposits as Reduction Agents on Iron Ore Using the Tar Impregnation Method

Ariany Zulkania ^{1,2}, Rochmadi Rochmadi ¹, Rochim Bakti Cahyono ¹ and Muslikhin Hidayat ^{1,*}

¹ Department of Chemical Engineering, Faculty of Engineering, Universitas Gadjah Mada, Jl. Grafika No. 2, Yogyakarta 55281, Indonesia; ariany.zulkania@mail.ugm.ac.id (A.Z.); rochmadi@ugm.ac.id (R.R.); rochimbakti@ugm.ac.id (R.B.C.)

² Department of Chemical Engineering, Faculty of Industrial Technology, Universitas Islam Indonesia, Jl. Kaliurang Km. 14.5, Yogyakarta 55584, Indonesia

* Correspondence: mhidayat@ugm.ac.id; Tel.: +62-815-7815-4093

Abstract: Increasing carbon deposits in iron ore to upgrade the reduction rate can be performed by impregnating iron ore in tar. Carbon containing iron ore was prepared from low-grade iron ore and biomass tar, which was generated from palm kernel shell (PKS) pyrolysis using the impregnation method. The optimum condition of the method was investigated by varying the tar-iron ore ratio (1 and 1.5) and impregnation time (0 and 24 h). After the carbonization of the tar-iron ore mixture in a flow-type quartz tubular fixed-bed reactor at 500 °C for an hour, the carbon deposits adhered well to surfaces of all iron ore samples. The carbon deposits increased when the ratio of tar-iron ore was enhanced. The effect of impregnation time on the formed carbon deposit only applied to the tar-iron ore ratio of 1, but it had a weak effect on the ratio of 1.5. The highest carbon content was obtained from the impregnation of a biomass tar-iron ore mixture with the ratio of 1.5 which was directly carbonized. In addition, the high water content of biomass tar affected the reformation of FeOOH at the impregnation within 24 h. Furthermore, the reduction reactivity of the obtained carbonized ore, which was observed using thermogravimetric analysis, was perceptible. The carbon deposits on iron ore were able to demote total weight loss up to 23%, compared to 8% of the dehydrated ore, during the heating process to 950 °C. The carbon content obtained from iron ore impregnation with biomass tar can act as reduction agents, thereby enhancing the reduction reactivity.



Citation: Zulkania, A.; Rochmadi, R.; Cahyono, R.B.; Hidayat, M. Investigation into Biomass Tar-Based Carbon Deposits as Reduction Agents on Iron Ore Using the Tar Impregnation Method. *Metals* **2021**, *11*, 1623. <https://doi.org/10.3390/met11101623>

Academic Editor: Alexander McLean

Received: 7 September 2021

Accepted: 7 October 2021

Published: 13 October 2021

Publisher's Note: MDPI stays neutral with regard to jurisdictional claims in published maps and institutional affiliations.



Copyright: © 2021 by the authors. Licensee MDPI, Basel, Switzerland. This article is an open access article distributed under the terms and conditions of the Creative Commons Attribution (CC BY) license (<https://creativecommons.org/licenses/by/4.0/>).

Keywords: biomass tar; carbon deposits; direct reduction; impregnation; iron ore; pyrolysis

1. Introduction

The iron-making industry is a contributor to global carbon emissions. Therefore, strategies in iron ore processing are needed to lessen the effect of CO₂ emission. One strategy that can be undertaken is to partially substitute fossil fuels with renewable fuels, one of which is sustainably sourced biomass. Related studies have revealed that biomass has a role in reducing CO₂ emissions from iron-making processes [1–4]. The biomass can act as a reduction agent in the iron ore reduction process, which are in the forms of carbon, CO, and H₂ yielded from the pyrolysis process [5–9]. When the tar vapor resulting from pyrolysis meets the surface of iron ore, it will be decomposed to generate gases, volatile matters, and carbon deposits. Simultaneously, the iron ore reduction will be driven [10].

The integration of biomass pyrolysis-iron ore reduction has provided a positive synergy for both processes. Iron ore affords to be a good catalyst for biomass tar being decomposed to volatile matter, gasses, and carbon deposit [10,11]. In addition, the integration can reduce the decomposition temperature of biomass/tar. Carbon, one of results of tar decomposition, lays in direct contact with the iron ore surfaces both on the outer surface and in the pores. Consequently, the reduction rate of iron ore is becoming faster [10–13].

This suggests that the direct reduction reaction will be more effective as the contact distance of carbon and iron ore is in nanoscale spacing. Chemical vapor infiltration (CVI) is a method utilized to produce carbon deposits on the surface of iron ore/carbonized ore. Tar vapor generated from the pyrolysis/gasification process will infiltrate the pores and further decompose into carbon, gases, and volatile matter once it contacts the iron ore's surfaces [11,14,15]. Related studies have shown that the utilization of vapor coal tar for the carbon deposited ore formation using the CVI method obtains carbon deposits of up to 12.7% mass for low-grade coal (LGC) at a vapor deposition temperature of 600 °C and 18% mass for coke oven gas (COG) at a tar pyrolysis temperature and a vapor deposition temperature of 700 and 350 °C, respectively, for a heating treatment time of 180–240 min. Whereas, the carbon deposit from biomass (PKS) tar vapor using the same method is lower, which is approximately 11.5% at a vapor deposition temperature of 600 °C [14,16]. The CVI method for carbon deposition in iron ore conducted by Zhao et al. [9] employed lignite blended with corn straw (1:1) as the reduction agent source. At a co-pyrolysis temperature and tar decomposition–carbon deposition temperatures of 600 °C and 650 °C, respectively, the carbon deposit acquired attained 10.92% mass.

Mochizuki et al. [15] elaborated a method of impregnating iron ore in COG tar and, subsequently, pyrolyzed the admixture at a temperature of 500 °C with a heating rate of 10 °C/min. The composite results indicated a higher carbon deposit reaching up to 22% mass. The high carbon deposit obtained from the tar impregnation method as performed by Mochizuki et al. [15] also ensued from an investigation carried out by Abe et al. [11] who used viscous coal tar blended with toluene which achieved 24.4% carbon mass. After the aforementioned tar impregnation studies, research continued looking into the reduction process. It showed that a greater amount of carbon deposits in carbonized ore increased the reduction reaction rate [11,15]. Ultimately, it delivered a higher reduction degree. This confirmed that the method of iron ore impregnated in tar is quite promising in providing carbon deposits within iron ore in connection with the supply of reduction agents for the direct reduction process. Furthermore, the utilization of carbon-containing iron ore from the tar impregnation process in iron-making industries is very attractive. Based on a study conducted by Suopajarvi [2], the use of carbon composite agglomerations (CCAs) gives beneficial in the blast furnace process, because it can reduce the reduction equilibrium temperature. Carbon composite agglomerations can accelerate the reduction and gasification reactions. In addition, CCAs can also be employed in the electric arc furnace (EAF) steel-making and direct reduced iron (DRI) production.

Based on prospective proceeds in the previous studies of tar impregnation and lack of information on the utilization of biomass tar as an impregnating agent, an integration involving tar decomposition and carbon deposition through the impregnation method of iron ore in the biomass tar, which was generated from palm kernel shell (PKS) pyrolysis, was proposed. To obtain the optimum condition for preparing carbon-containing iron ore, composites/carbonized ore results were examined for their carbon content based on the variation of biomass tar to iron ore ratios and impregnating times. Furthermore, the characteristics and composition of the composites were also investigated. Eventually, the effect of the carbon deposit of the composite on the reduction reactivity was verified using thermogravimetric analysis.

2. Materials and Methods

2.1. Materials

Dehydrated ores were prepared from goethite ores supported by PT. Meratus Jaya Iron&Steel, South Kalimantan, Indonesia, with sizes ranging from 1 to 3 cm. The goethite ores were then ground and screened into particle sizes from 53 to 150 µm. Before being used in the carbonization process, they were heated in a furnace at 350 °C with a heating rate of 3.5 °C/min for 3 h in an air atmosphere to eliminate combined water (CW) and enhance the surface area of the samples. Additionally, biomass tar was recovered from pyrolysis of waste PKS supplied by PT. Astra Agro Lestari Tbk., Jakarta, Indonesia, where

the pyrolysis was conducted at a temperature of 500 °C for an hour under N₂ gas flow. Before being used for the impregnation process, the tar was separated from the aqueous phase using centrifugation. To observe the reactivity of carbonized ore obtained using thermogravimetric analysis, molasses was used as a binder in the formation of pellets by 9% mass. Thin cylinder pellets with a diameter of 2 mm and a composite weight of 19 mg were made using pellet mold and a pressure of 2 kN (hydraulic pump). Further, they were dried in an oven at 105 °C for 3 h to remove moisture and stored in a closed bottle before utilizing.

2.2. Preparation of Carbon-Containing Iron Ores

The carbon-containing ore composites were prepared using an apparatus set as displayed in Figure 1. After the dehydrated ores were charged into an alumina crucible, the biomass tar was added to the crucible. To obtain optimum impregnation conditions, the composites were prepared with the different tar-ore ratios of 1 and 1.5 (mL/g). A study conducted by Mochizuki et al. [15] denoted that the ratio of the COG tar-iron ore ranging from 1 to 3 in the impregnation method gave carbon deposits approximately in the range of 17–25%. Besides, the carbon deposit formation was evidenced by the dramatically reduced pore surface area at a ratio of 1, which was 1 m²/g from 40 m²/g of the dehydrated ores and further decreased to around zero at ratios of 1.5 until 3. After the mixture of each ratio was physically stirred, it was then subjected to two methods of impregnation time. The first and second methods were the mixture was immediately put in a flow-type quartz tubular fixed-bed reactor to be carbonized and the mixture was left for 24 h at room temperature before being put in the reactor for carbonization, respectively. Further, the tar-ores mixture was calcined at 500 °C for an hour with a heating rate of 10 °C/min under N₂ gas flow (50 mL/min). The largest carbon deposit formed from the carbonization process based on the study performed by Rozhan et al. [13] was obtained at 500 °C instead of at 600 and 700 °C. Additionally, Cahyono et al. [17] stated that tar carbon deposition within the porous ore was paramount in the temperature range of 400–600 °C. The obtained composites were then crushed into sizes of 53–150 µm particles. Potential carbonized ores were the ones having the most carbon deposits.

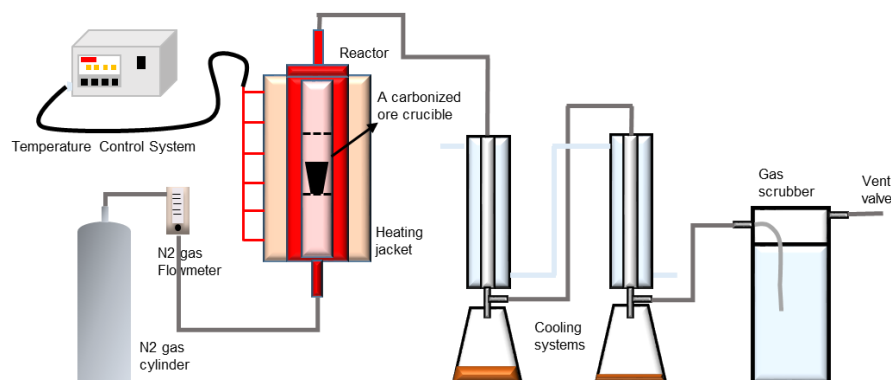


Figure 1. Scheme of the apparatus for carbonization process.

2.3. Characterization

Composition and phase identification of the original iron ore/goethite were analyzed utilizing X-ray fluorescence (XRF Epsilon 4, Malvern Panalytical Ltd., Malvern, UK) and X-ray diffraction (XRD-Bruker D2 Phaser, Bruker Corporation, Billerica, MA, USA) and are listed in Table 1.

Table 1. Composition of original iron ore.

Composition	TFe	Fe ₂ O ₃	Si	Ca	Al	O	CW	C
Weight (mass%)	46.835	18.941	9.225	5.366	0.534	37.492	4.93	5.62

TFe: total Fe; CW: combined water.

The XRD analysis was also conducted on the dehydrated ore and the carbonized ores. Components and the amount of carbon in the biomass tar and ores were determined using proximate analysis (Nabertherm N3/R Muffle furnace, Nabertherm GmbH, Lilienthal, Germany; Heraeus UT 5042 EK, Labexchange, Burladingen, Germany) conducted at The Center for Food and Nutrition Studies Laboratory, Gadjah Mada University, Yogyakarta, Indonesia, and elemental analysis (CHN/S-628/632, LECO Corporation, St. Joseph, MI, USA) conducted at The Research and Development Center for Mineral and Coal Technology, Jakarta, Indonesia. The results of both analyses of the PKS tar are denoted in Table 2. Dispersed water in the biomass tar was quite high, up to 69.5%, and comparable to those of other studies [18,19]. The small amount of fixed carbon compared with that of the volatile matter and the high water content indicated that the biomass tar was low-grade tar with its utilization as a carbon provider in the tar impregnation method. Moreover, the low carbon content of 60.73% by mass also indicates similar tar quality when compared to the COG tar's carbon content of 91% by mass [15].

Table 2. Properties of the biomass tar.

Proximate Analysis (Mass%, Air-Dried Basis)				Ultimate Analysis (Mass%, Air-Dried Basis)				
Fixed Carbon	Volatile Matter	Water	Ash	C	H	O	N	S
9.261	21.124	69.551	0.064	60.730	7.800	0.450	30.946	0.074

The surface structure and chemical characteristics of all solid samples were observed using scanning electron microscopy (SEM-Jeol Jsm 6510 La, JEOL Ltd., Tokyo, Japan) equipped with energy-dispersive X-ray spectroscopy (EDS) and mapping. The pore distribution, pore-volume, and BET surface area were determined by N₂ adsorption–desorption measurements (Quantachrome Instr. Ver. 10.01, Anton Paar Comp., Boynton Beach, FL, USA). Finally, the reduction reactivity of the obtained carbonized ores was observed by the thermogravimetric method (TG-Linseis STA, Linseis Messgeraete GmbH, Selb, Germany).

3. Results and Discussion

3.1. Tar Impregnation and Carbon Deposition

The effect of tar impregnation on the carbon content changes of iron ore is illustrated in Figure 2. The C contents that existed in the original iron ore decreased after the dehydration step. They were released as CO and/or CO₂ when heated [13], implying the removal of oxygen upon heating when it was associated with iron oxide. The carbon deposits were prepared using biomass tar impregnation process which the ratio of tar-dehydrated iron ore was varied to 1.5 and 1 (mL/g). To probe the impregnation time effect, each ratio was then split into samples that were immediately carbonized (D1 and D3) and ones that were impregnated for 24 h before carbonization (D2 and D4), respectively. Based on the elemental analysis, the carbon content of dehydrated ores significantly enhanced after both impregnation and carbonization processes.

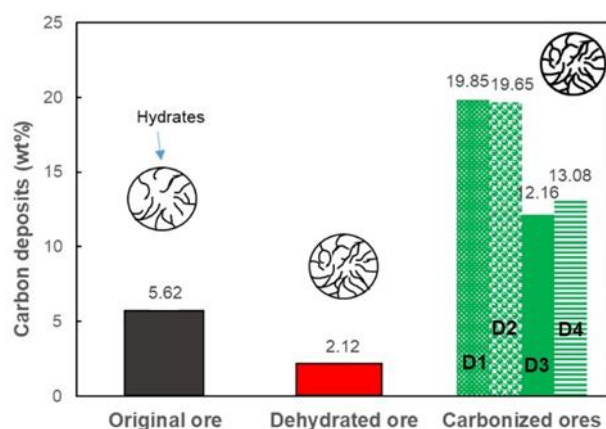
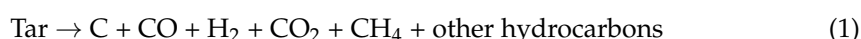
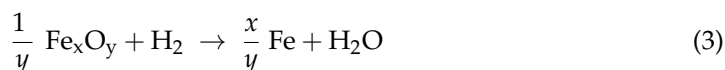
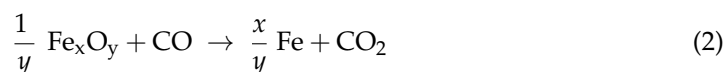


Figure 2. Carbon deposit changes of the samples: original ore (before dehydration), dehydrated ore, and carbonized ores (D1, D2, D3, and D4).

During the carbonization at 500 °C for 1 h under the N₂ flow, the tar was decomposed according to the following reaction [14]:



Due to the impregnation, before achieving the pyrolysis temperature, a portion of the tar infiltrated into the pores and adsorbed on the iron surface. When the pyrolysis process occurred, the carbon produced as in the Reaction (1) established deposits on the surfaces [13,17]. Simultaneously, the resulting gases encouraged the indirect reduction if they came into contact with the carbon-free iron surfaces [10] following these reactions:

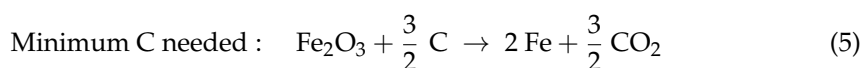
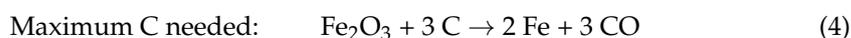


Based on the investigation conducted by Cahyono et al. [10], the Fe–O–C phase diagram based on the CO/(CO+CO₂) ratio exhibited that the reduction at temperatures below 560 °C could occur gradually by the following route: Fe₂O₃ → Fe₃O₄ → Fe. Furthermore, Mochizuki et al. [15] studied the impregnation of iron ore in the COG tar which was continued carbonization at a temperature of 500 °C and a heating rate of 10 °C/min. The XRD analysis of the carbon composites' results showed the presence of Fe₃O₄ compounds other than Fe₂O₃. This indicated that reduction of Fe₂O₃ → Fe₃O₄ took place slowly during the heating process.

By using the impregnation method, the biomass tar significantly increased carbon deposits by 12.16–19.85% dry mass at both the tar-iron ore ratios of 1 and 1.5. The result was quite comparable with the investigation performed by Mochizuki et al. [15] where carbon deposits generated from COG tar impregnation were approximately 17–22% dry mass for the tar-iron ore ratio of 1:1.5. Furthermore, it is reflected from Figure 2 that increasing the tar-iron ore ratio from 1 to 1.5 lead to the escalation of carbon deposits from 12.16–13.08% to 19.65–19.85%, respectively. This is following the statement from Mochizuki et al. [15] that increasing the tar-iron ore ratio could enhance the carbon deposits. On the other hand, the effect of the impregnation time on carbon deposits obtained gave a different trend for each ratio. The tar-iron ore ratio of 1 (D3 and D4) showed that longer impregnation time afforded larger carbon deposits, meanwhile the ratio of 1.5 (D1 and D2) indicated that the carbon deposits of the 24 h impregnation were slightly less to the ones of impregnation that immediately carbonized. The impregnation insisted the tar infiltrating to the pores, after which the tar was decomposed resulting in carbon deposition, volatile matter, and gases during the heating process/carbonization. The tar impregnation time of 24 h ensured that carbon deposition was larger compared to the shorter timeframe and was reflected in the

tar-iron ore ratio of 1. Nevertheless, when the amount of tar liquid was increased to a ratio of 1.5, the effect of impregnation time was insignificant to the carbon deposition, which can be seen by noticing that the carbon deposits of both impregnation methods were almost the same as reflected in D1 and D2. In addition, in the heating process during the carbonization, three reaction mechanisms took place simultaneously including a reduction in the presence of CO and H₂ gases, carbon deposition, and carbon consumption [9]. The carbon deposition rate in both impregnation time methods indicated almost the same since they were carried out under the same operating conditions. Nevertheless, the carbon consumption rate in D2 seemed slightly higher than that in D1, inducing the carbon deposits of D2 was slightly less than those of D1.

Based on the iron ore composition in Table 1, the total Fe of the sample was 46.835%. Theoretically, the amount of carbon required for iron reduction could be calculated according to the Equations (4) and (5) using the Fe value as previously mentioned and assuming that all the iron contained in the sample was Fe₂O₃ [13]:



The maximum and minimum carbon needed for directly reducing the iron sample are 15.096 and 7.548 %mass, respectively. From the experiment, D1 and D2 contained carbon deposits more than the maximum carbon needed for iron reduction, namely, 19.85 and 19.65 %mass, respectively. Accordingly, both carbonized ores are possibly directly reduced to iron.

Carbon-containing ores were prepared from the calcined goethite ores. The goethite ores mainly contained FeOOH before being dehydrated and were significantly decomposed to Fe₂O₃ by following reaction [11,14]:



The study performed by Saito et al. [20] exhibited that the optimum temperatures for the goethite ores dehydration were in the range of 230–400 °C, which is where the high surface areas were formed. The FeOOH began to dehydrate at 230 °C, forming ~4 nm nanopores. After dehydrating above 400 °C, the surface area started decreasing. Additionally, Abe et al. [11] suggested that the pore structure type of the goethite calcined at a temperature of 300–500 °C had a pore size of 2–4 nm. The changes in pore size distribution, Brunauer–Emmett–Teller (BET) surface area, and pore volumes of goethite ore, dehydrated ore, and carbonized ores are represented in Figure 3. All four samples tend to have nanopores at approximately 2 nm. After the release of bound water due to the heating process, the nanopores increased in the dehydrated sample as well as the mesopores at a size of 2–13 nm. The availability of nanopores is favorable for forming carbon deposits during tar decomposition [14,21]. The carbon deposit derived from tar impregnation and, subsequently, the carbonization process was able to reduce the pore size distribution and specific surface area of the dehydrated ores [15,21]. Figure 3a reveals that the carbon deposition-covered nanopores and mesopores of D1 were higher compared to sample D2, which is indicated by the pore distribution of nanopores and mesopores of D1 was lower. Moreover, there were still vacant nanopores and mesopores in the D2 sample unlike D1. This was induced by the presence of tar staying longer in impregnation, which causes more clogging on the surface of the iron ore. Therefore, even though the surface area differences of both carbonized ores were very small, the pore volume of D2 exhibited a higher level than D1 as shown in Figure 3b.

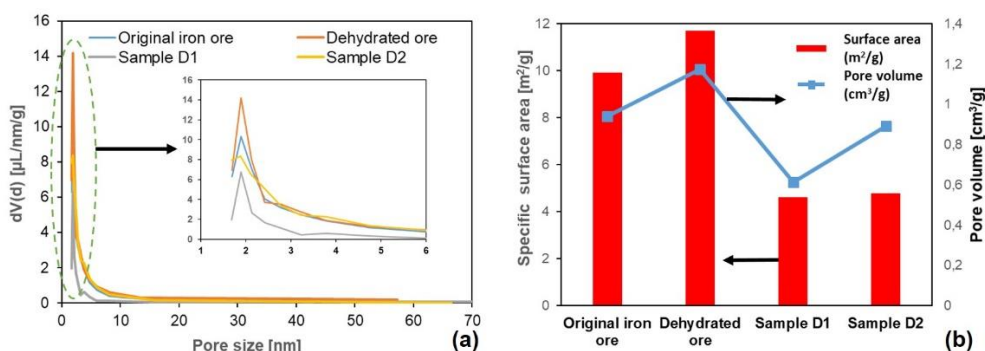


Figure 3. Changes in (a) pore size distribution; (b) S_{BET} and V_{BJH} values of original iron ore, dehydrated ore, and D1 and D2 samples. (S_{BET} : Brunauer, Emmett and Teller (BET) Specific Surface Area; V_{BJH} : Barrett-Joyner-Halenda (BJH) pore volume).

Surface morphology changes in the samples (before and after dehydrating) were observed using SEM-EDX illustrated in Figure 4. Figure 4a reflects that the goethite is significantly contained in the original ore sample which is depicted by characteristic needle-shaped bulges [9,22,23] and colloform texture with cavities of goethite [8] shown by the red circles. It seems that the needle and colloform surfaces are smooth and neither scratches nor grooves are to be seen, indicating that the combined water and gangues were distributed in the goethite samples. After dehydrating, the iron ore surface morphology dramatically changed as shown in Figure 4b. Porous structures are visible in the heated samples because of the water removal following the Equation (6) and the removal of oxygen associated with iron oxide. The surface looks coarse and grained with hexagonal and cubic shapes, exhibiting the presence of iron oxides such as hematite and magnetite, respectively [24].

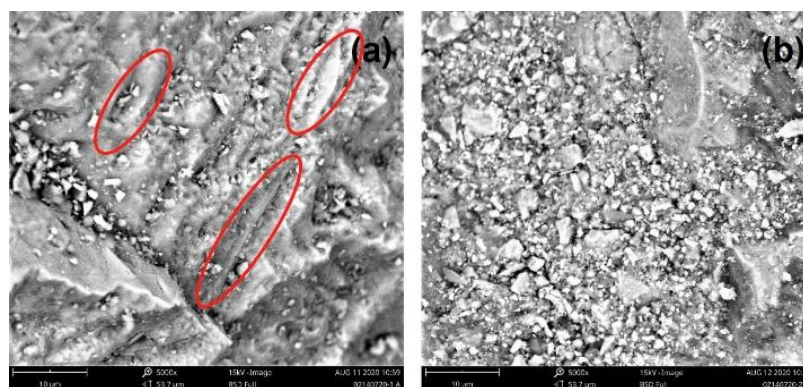


Figure 4. SEM images showing a change in the iron ore surface after dehydration: (a) iron ore before dehydration; (b) iron ore after dehydration. Red circles show needle-shaped bulges and colloform texture with cavities of goethite.

The surface morphology of the dehydrated ore after carbonization (carbonized ore) is denoted in Figure 5. From Figure 5a,c, it seems that the thick layers of carbon spread on both iron sample surfaces were almost the same, which corresponds with the surface areas for both D1 and D2 as reflected in Figure 3b. The coarse and grained surfaces of dehydrated ores are almost fully covered by carbon. However, the carbon element of D1 was higher compared to that of D2 based on intensity height as shown in Figure 5b,d. In addition, as represented in Figure 3b, the average pore volume of D1 was also lower than those of D2, indicating that the carbon deposition rate in D1 was higher than that of D2. It confirmed that the carbon deposits of D1 were slightly larger than those of D2 as reflected in Figure 2.

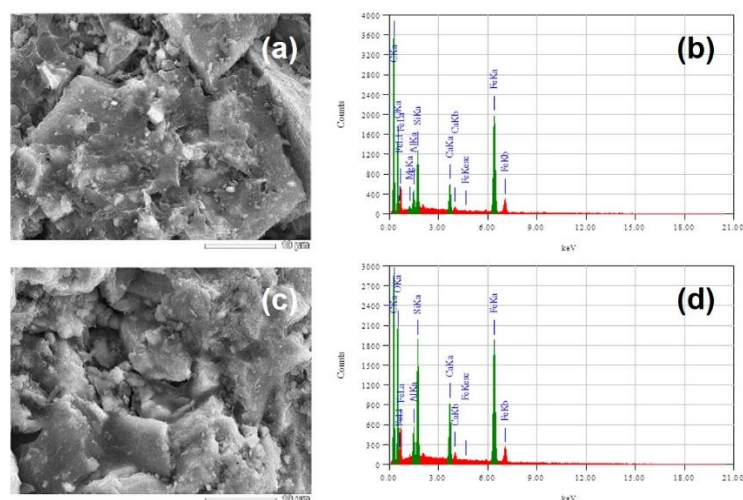


Figure 5. SEM images showing a change in iron ore surfaces after carbonization of impregnated ore and the results of EDX analyses: (a,b) Sample D1, (c,d) Sample D2.

Carbonaceous material distribution in the carbonized ore was observed using SEM-EDX-mapping. The carbon, Fe, and oxygen mapping results are denoted in Figure 6. From the figures, it reveals that Fe-element, in red areas, was uniformly presented in the dehydrated samples with measly carbon and oxygen presences (Figure 6a). On the other hand, the amount of carbon formed in the carbonized ores, by comparing to the dehydrated ore, was significant. It is reflected in Figure 6b,c where the C-element's presence, in green areas,- was quite dominant. This investigation shows that the carbonaceous materials derived from the biomass tar were infiltrated into the pores and adsorbed onto the iron ore's surfaces during the impregnation process and, subsequently, the tar was decomposed as per Equation (1) at pyrolysis temperature, which led to carbon deposits covering the surfaces. However, it appears that the carbon-covered surface on D1 was broader than that of D2, exhibiting that the carbon deposit of D1 was slightly higher than the one of D2. This corresponds with the trend depicted in Figure 5b,d.

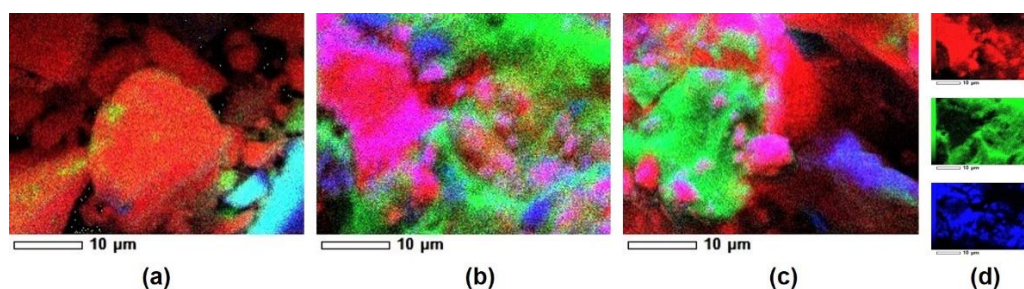


Figure 6. Elemental mapping of C-element: (a) dehydrated ore, (b) Sample D1, (c) Sample D2, and (d) red, green, and blue areas corresponding to Fe-, C-, and O-elements, respectively.

3.2. Characteristic and Composition of Carbon-Containing Iron Ore

Characteristics of the ore structures before and after the impregnation and carbonization process were analyzed using X-ray diffractometry (XRD). It was conducted for the original ore, the dehydrated ore, and two carbonized ores with the greater carbon deposits (D1 and D2); the XRD pattern of them are exhibited in Figure 7. It can be seen that the original ore mainly had FeOOH content. Mostly, FeOOH peaks disappeared after the dehydration process at 350 °C for three hours with a heating rate of 3.5 °C/min under the N₂ flow. In addition, the appearance of the peaks of Fe₂O₃ and Fe₃O₄ increased, indicating that the FeOOH transformed into Fe₂O₃ and further to Fe₃O₄. For carbonized ore samples,

most of Fe_2O_3 disappeared transforming into Fe_3O_4 in D1. This possibly happens since the gas-produced from the tar pyrolysis encourages the reduction process to occur as Equations (2) and (3). Meanwhile, in D2, the existence of Fe_2O_3 and Fe_3O_4 was almost the same. Surprisingly, an interesting phenomenon occurred in D2 where the presence of FeOOH increased. It could be due to the significant amount of water adsorbed on the dehydrated ore surfaces during the impregnation for 24 h. As described in Table 2, the water contained in the biomass tar is quite high (up to 69%). Otherwise, the carbonized ore resulting from coke oven gas (COG) tar impregnation exhibited a different phenomenon [15]. Since the COG tar had high C content (up to 91%) and almost no water [25], the FeOOH did not appear in the carbonized ore.

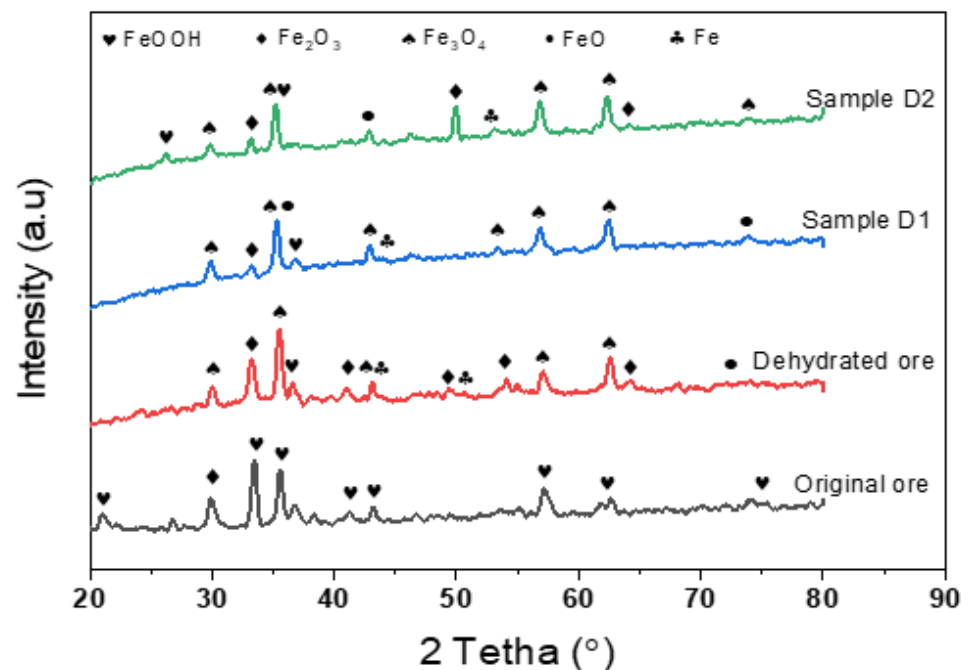


Figure 7. XRD (X-ray diffractometry) pattern of samples before and after the carbonization process at 500 °C for 1 h.

The composition of the ore samples before and after the carbonization process is displayed in Figure 8. Mass fraction of iron oxide component was adapted from the reference intensity ratio (RIR) method which is based on the intensity of the X-ray diffracted by the component's specified plane (hkl) [11,26,27]. The original ore contained high amounts of FeOOH up to 67%. By heating, most of FeOOH were transformed into Fe_2O_3 as per Reaction (6). The heating process can slightly trigger reduction reactions $\text{Fe}_2\text{O}_3 \rightarrow \text{Fe}_3\text{O}_4 \rightarrow \text{FeO} \rightarrow \text{Fe}$. It corresponds with the XRD pattern as reflected in Figure 7. The reduction effect could be also contributed by the carbon content present in the original ore. This is confirmed by a decrease in the carbon content in the dehydrated ore as shown in Figure 2, where the carbon contents of the original and dehydrated ores were 5.62 and 2.12% by mass, respectively. This is in line with the study conducted by Rozhan et al. [13], which showed that the dehydration process caused a decline in the carbon content of the original ore, which was liberated as CO and/or CO_2 . In addition, from the XRD analysis of the dehydrated ore, it appears that there was a small portion of the Fe_3O_4 phase.

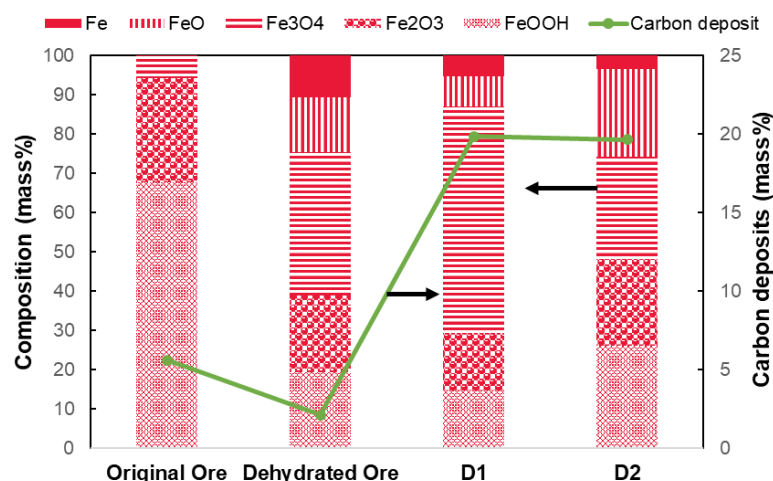
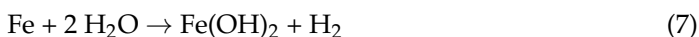


Figure 8. Composition and carbon deposits of the sample before and after tar impregnation and carbonization process. Carbonized ore D1: resulting from biomass tar impregnation which immediately carbonized; carbonized ore D2: resulting from biomass tar impregnation for 24 h before the carbonization process.

After the tar impregnation and carbonization process of the dehydrated ore, a different phenomenon occurred between D1 and D2. The amount of FeOOH, FeO, and Fe decreased, while the Fe₃O₄ increased in D1. The carbonization at 500 °C drove the transformation of FeOOH into Fe₂O₃ and further into Fe₃O₄. Gas resulting from tar gasification, such as CO and H₂, and carbon deposits produced from the biomass tar pyrolysis during carbonization could promote the reduction [10]. However, the high water content of the biomass tar could affect the iron oxide. The FeO and Fe laying on the outer surface of the ore fine particles had more opportunity to make contact with the water which could encourage the conversion of Fe to Fe(OH)₂ in an anaerobic condition based on the following reaction [28]:



and FeO to Fe(OH)₂ also based on the study performed by Rollason and Plane [29] and Zhao et al. [30]. Under the appropriate conditions of Fe (II) concentration, Fe(OH)₂ could be converted into goethite (FeOOH) [31]. Subsequently, FeOOH converted into Fe₂O₃ and further into Fe₃O₄ due to the reduction effect during the carbonization process.

Different conditions occurred in D2 during impregnation and carbonization. Compared to the dehydrated ore, the FeOOH and FeO contents increased while the Fe and Fe₃O₄ diminished, indicating that during impregnation for 24 h, the water of the biomass tar was significantly adsorbed on the surface of iron ore. As previously elucidated, Filip et al. [28] (2004) stated that Fe could convert into Fe(OH)₂ following Equation (7) in the anaerobic condition, and, further, it could be transformed into FeOOH [31]. Since more water was adsorbed on the D2 surfaces compared to the D1 ones, FeOOH formation was higher in D2. On the other hand, the biomass tar could also be infiltrated into the pores and adsorbed well on the iron ore surface for impregnation for 24 h. During the carbonization process, high temperature encouraged biomass tar decomposition resulting in C deposit, CO and H₂ gases, and some volatile matter, which subsequently promoted the reduction when they contacted the iron oxides surfaces. The effect of sufficient water and tar adsorption induced a slight complexity in D2. The FeOOH formation was higher compared to D1. However, the high reduction occurred due to the adequate availability of CO and H₂ gases and carbon deposits which revealed that the reduction was ensued for transforming Fe₃O₄ to FeO as shown in Figure 8. Eventually, based on the comparison, the method of tar impregnation which led to immediate carbonization (D1) will be utilized in the next reduction process, since it can generate slightly greater carbon deposits and less FeOOH content.

3.3. Reactivity of the Carbonized Ore in the Inert Atmosphere

The characteristics of the reduction reactivity of the carbonized ore were investigated using the thermogravimetric method of D1, which had the greater carbon deposits and the lowest FeOOH content. As seen in Figure 9, the carbonized ore was compared with the dehydrated ore to observe the effect of the carbon deposit on the reduction. The pellet formation process of both samples was assisted by the molasses as the binder by 9% mass due to the necessity for the TGA, which had fixed carbon, volatile matter, water content, and ash contents of 4.94%, 56.44%, 35.19%, and 3.43%, respectively.

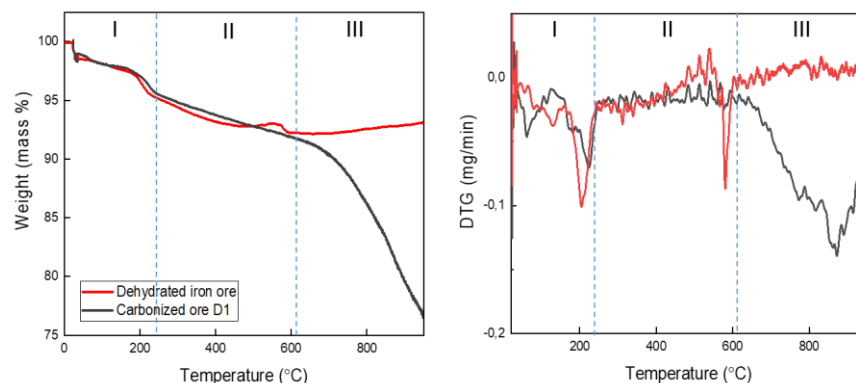
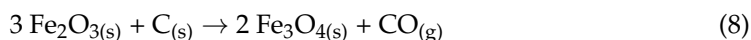


Figure 9. Comparison of the reactivity of carbonized ore and dehydrated ore using thermogravimetric analysis (TGA) with a heating rate of 10 °C/min under an N₂ atmosphere. The carbon contents of the carbonized ore and dehydrated ore were 19.85% and 2.12% (as shown in Figure 2), respectively. Symbols I, II, III denote first, second, and third stages of weight loss, respectively, in thermogravimetric analysis based on temperature changes.

The curve trends of both samples were almost the same at temperatures below 600 °C. The molasses content influenced the heating characteristic of the samples, where there was small weight loss at temperatures below 200 °C indicating an evaporation process of water content (stage 1). Figure 9 reveals that the first maximum weight loss peaks of both samples in the DTG curves were approximately at around 200 °C. Related studies notified that the first maximum peak of the biomass/fuel pyrolysis was around 100–350 °C attributing to the drying, dehydration, de-polymerization, and decomposition of the biomass/fuels [11,21,32]. However, for some pure iron ores and carbonized ore, there was almost no weight loss for temperatures less than 500 °C [21]. Furthermore, in the second stage at a temperature range of 250–610 °C, there was a small continuous weight loss indicating the volatile matter release and slow reduction process. The second maximum peak of the dehydrated ore emerged at around 600 °C representing the reduction that occurred, whereas the carbonized ore had a slow reduction process at this stage. Zuo et al. [33] stated that the first main reduction reaction occurred at a temperature range of 565–847 °C adhered to the following reaction:



which generated low valence iron oxide as the main reduction product, such as Fe₃O₄, and additionally, the CO gas produced was also able to contribute to Fe₂O₃ reduction. Hereinafter, the third stage was the reaction process at a temperature range of 610–950 °C, in which the dehydrated ore had almost no weight loss change evidencing very slow reduction taken place at this stage. Oppositely, in this stage, the carbonized ore started losing weight at around 610 °C for the reduction and, subsequently, the weight loss was becoming larger until reaching the second maximum peak at 850 °C as shown in Figure 9. The total weight loss ratio of the carbonized ore in this stage was 15%. The third stage was the stage of carbon gasification and CO gas reduction which is the most prominent of the reduction processes [33]. The TGA results shown in Figure 9 depict that the carbon deposit

of the carbon-containing iron ore significantly enhanced the reduction reactivity of the iron ore at a temperature around 850 °C. It is evidenced by its total weight loss of up to 23% in comparison to 8% of the dehydrated ore.

4. Conclusions

The conclusions of the study are summarized as follow:

1. Impregnation of iron ore with biomass tar continued via the carbonizing process produced a carbon layer on the iron ore's surface. When the tar-iron ore ratio was enhanced, the carbon deposit increased as well. It was shown that the ratio of 1 gave a carbon deposit of 12.16–13.08% by mass, while the ratio of 1.5 gave a carbon content of 19.65–19.85% mass. The nanopores of the dehydrated ore encouraged the formation of nanocontact between the tar and iron ore;
2. The longer impregnation process raised the carbon deposit at the biomass tar-iron ore ratio of 1. However, the impregnation time did not have a major effect on carbon deposition at the ratio of 1.5;
3. The high water content of biomass tar affected the composition of iron compounds in the carbon-containing iron ore, where the longer impregnation time re-formed the FeOOH compounds. D2, which was impregnated for 24 h, exhibited increases in the FeOOH content compared to the dehydrated ore.
4. The formation of carbon deposits in iron ore increased the reduction rate of iron ore during a rise in temperature of up to 950 °C. This was confirmed by a decrease in total weight loss of carbonized ore of up to 23% mass compared to dehydrated ore which was 8% mass;
5. The promising prospect of utilizing the method of impregnating iron ore in tar in terms of providing iron ore–carbon composites can be motivation for development in the iron-making industry. The provision of pre-treatment units, namely, processes of tar impregnation and carbonization before the reduction process of the iron–carbon ore composites, is expected to lower the temperature of the reduction process which leads to energy savings.

Author Contributions: Conceptualization, M.H., R.R., R.B.C. and A.Z.; methodology, M.H., R.R., R.B.C. and A.Z.; software, M.H., R.R. and A.Z.; validation, M.H., R.R. and R.B.C.; formal analysis, R.B.C. and A.Z.; investigation, A.Z.; resources, A.Z.; data curation, A.Z.; writing—original draft preparation, A.Z.; writing—review and editing, M.H., R.R. and R.B.C.; visualization, A.Z.; supervision, M.H., R.R. and R.B.C.; project administration, A.Z.; funding acquisition, M.H. and R.B.C. All authors have read and agreed to the published version of the manuscript.

Funding: This research and the APC was funded by “Direktorat Jenderal Penguatan Riset dan Pengembangan, Kementerian Riset, Teknologi, dan Pendidikan Tinggi” with grant number: 2307/UN1/DITLIT/DITLIT/PT/2021.

Institutional Review Board Statement: Not Applicable.

Informed Consent Statement: Not Applicable.

Data Availability Statement: The data presented in this study are available on request from the corresponding author.

Acknowledgments: The author would like to thank to “Direktorat Jenderal Penguatan Riset dan Pengembangan, Kementerian Riset, Teknologi, dan Pendidikan Tinggi” for the research funding. For additional support, the following companies are acknowledged: PT. Meratus Jaya Iron&Steel, South Kalimantan, Indonesia, and PT. Astra Agro Lestari Tbk., Indonesia.

Conflicts of Interest: The authors declare no conflict of interest.

References

1. Mousa, E.; Wang, C.; Riesbeck, J.; Larsson, M. Biomass applications in iron and steel industry: An overview of challenges and opportunities. *Renew. Sustain. Energy Rev.* **2016**, *65*, 1247–1266. [\[CrossRef\]](#)
2. Suopajarvi, H.; Kemppainen, A.; Haapakangas, J.; Fabritius, T. Extensive review of the opportunities to use biomass-based fuels in iron and steelmaking processes. *J. Clean. Prod.* **2017**, *148*, 709–734. [\[CrossRef\]](#)
3. Purwanto, H.; Zakiyuddin, A.M.; Rozhan, A.N.; Mohamad, A.S.; Salleh, H.M. Effect of charcoal derived from oil palm empty fruit bunch on the sinter characteristics of low grade iron ore. *J. Clean. Prod.* **2018**, *200*, 954–959. [\[CrossRef\]](#)
4. Ubando, A.T.; Chen, W.-H.; Ong, H.C. Iron oxide reduction by graphite and torrefied biomass analyzed by TG-FTIR for mitigating CO₂ emissions. *Energy* **2019**, *180*, 968–977. [\[CrossRef\]](#)
5. Cheng, Z.; Yang, J.; Zhou, L.; Liu, Y.; Guo, Z.; Wang, Q. Experimental study of commercial charcoal as alternative fuel for coke breeze in iron ore sintering process. *Energy Convers. Manag.* **2016**, *125*, 254–263. [\[CrossRef\]](#)
6. Huang, D.-B.; Zong, Y.-B.; Wei, R.; Gao, W.; Liu, X.-M. Direct Reduction of High-phosphorus Oolitic Hematite Ore Based on Biomass Pyrolysis. *J. Iron Steel Res. Int.* **2016**, *23*, 874–883. [\[CrossRef\]](#)
7. Wei, R.; Cang, D.; Bai, Y.; Huang, D.; Liu, X. Reduction characteristics and kinetics of iron oxide by carbon in biomass. *Ironmak. Steelmak.* **2016**, *43*, 144–152. [\[CrossRef\]](#)
8. Nayak, D.; Dash, N.; Ray, N.; Rath, S.S. Utilization of waste coconut shells in the reduction roasting of overburden from iron ore mines. *Powder Technol.* **2019**, *353*, 450–458. [\[CrossRef\]](#)
9. Zhao, H.; Li, Y.; Song, Q.; Liu, S.; Ma, Q.; Ma, L.; Shu, X. Catalytic reforming of volatiles from co-pyrolysis of lignite blended with corn straw over three different structures of iron ores. *J. Anal. Appl. Pyrolysis* **2019**, *144*, 104714. [\[CrossRef\]](#)
10. Cahyono, R.B.; Rozhan, A.N.; Yasuda, N.; Nomura, T.; Hosokai, S.; Kashiwaya, Y.; Akiyama, T. Catalytic coal-tar decomposition to enhance reactivity of low-grade iron ore. *Fuel Process. Technol.* **2013**, *113*, 84–89. [\[CrossRef\]](#)
11. Abe, K.; Kurniawan, A.; Ohashi, K.; Nomura, T.; Akiyama, T. Ultrafast Iron-Making Method: Carbon Combustion Synthesis from Carbon-Infiltrated Goethite Ore. *ACS Omega* **2018**, *3*, 6151–6157. [\[CrossRef\]](#)
12. Hata, Y.; Purwanto, H.; Hosokai, S.; Hayashi, J.-I.; Kashiwaya, Y.; Akiyama, T. Biotar Ironmaking Using Wooden Biomass and Nanoporous Iron Ore. *Energy Fuels* **2009**, *23*, 1128–1131. [\[CrossRef\]](#)
13. Rozhan, A.N.; Cahyono, R.B.; Yasuda, N.; Nomura, T.; Hosokai, S.; Akiyama, T. Carbon Deposition of Biotar from Pine Sawdust by Chemical Vapor Infiltration on Steelmaking Slag as a Supplementary Fuel in Steelworks. *Energy Fuels* **2012**, *26*, 3196–3200. [\[CrossRef\]](#)
14. Cahyono, R.B.; Rozhan, A.N.; Yasuda, N.; Nomura, T.; Purwanto, H.; Akiyama, T. Carbon Deposition Using Various Solid Fuels for Ironmaking Applications. *Energy Fuels* **2013**, *27*, 2687–2692. [\[CrossRef\]](#)
15. Mochizuki, Y.; Nishio, M.; Tsubouchi, N.; Akiyama, T. Reduction Rate and Crushing Strength of a Carbon-Containing Pellet Prepared by the Impregnation Method of COG Tar. *Energy Fuels* **2016**, *30*, 2102–2110. [\[CrossRef\]](#)
16. Mochizuki, Y.; Nishio, M.; Tsubouchi, N.; Akiyama, T. Preparation of a Carbon-Containing Pellet with High Strength and High Reactivity by Vapor Deposition of Tar to a Cold-Bonded Pellet. *Energy Fuels* **2017**, *31*, 8877–8885. [\[CrossRef\]](#)
17. Cahyono, R.B.; Yasuda, N.; Nomura, T.; Akiyama, T. Optimum temperatures for carbon deposition during integrated coal pyrolysis–tar decomposition over low-grade iron ore for ironmaking applications. *Fuel Process. Technol.* **2014**, *119*, 272–277. [\[CrossRef\]](#)
18. Chen, D.; Zhou, J.; Zhang, Q. Effects of heating rate on slow pyrolysis behavior, kinetic parameters and products properties of moso bamboo. *Bioresour. Technol.* **2014**, *169*, 313–319. [\[CrossRef\]](#) [\[PubMed\]](#)
19. Sakulkit, P.; Palamanit, A.; Dejchanchaiwong, R.; Reubroycharoen, P. Characteristics of pyrolysis products from pyrolysis and co-pyrolysis of rubber wood and oil palm trunk biomass for biofuel and value-added applications. *J. Environ. Chem. Eng.* **2020**, *8*, 104561. [\[CrossRef\]](#)
20. Saito, G.; Nomura, T.; Sakaguchi, N.; Akiyama, T. Optimization of the Dehydration Temperature of Goethite to Control Pore Morphology. *ISIJ Int.* **2016**, *56*, 1598–1605. [\[CrossRef\]](#)
21. Zhao, H.; Li, Y.; Song, Q.; Liu, S.; Ma, L.; Shu, X. Catalytic reforming of volatiles from co-pyrolysis of lignite blended with corn straw over three iron ores: Effect of iron ore types on the product distribution, carbon-deposited iron ore reactivity and its mechanism. *Fuel* **2021**, *286*, 119398. [\[CrossRef\]](#)
22. Walter, D.; Buxbaum, G.; Laqua, W. The Mechanism of the Thermal Transformation From Goethite to Hematite. *J. Therm. Anal. Calorim.* **2001**, *63*, 733–748. [\[CrossRef\]](#)
23. Pradhan, N.; Nayak, R.R.; Mishra, D.K.; Priyadarshini, E.; Sukla, L.B.; Mishra, B.K. Microbial Treatment of Lateritic Ni-ore for Iron Beneficiation and Their Characterization. *World Environ.* **2012**, *2*, 110–115. [\[CrossRef\]](#)
24. Wei, Z.; Zhang, J.; Qin, B.; Dong, Y.; Lu, Y.; Li, Y.; Hao, W.; Zhang, Y. Reduction kinetics of hematite ore fines with H₂ in a rotary drum reactor. *Powder Technol.* **2018**, *332*, 18–26. [\[CrossRef\]](#)
25. Miura, K.; Kawase, M.; Nakagawa, H.; Ashida, R.; Nakai, T.; Ishikawa, T. Conversion of Tar in Hot Coke Oven Gas by Pyrolysis and Steam Reforming. *J. Chem. Eng. Jpn.* **2003**, *36*, 735–741. [\[CrossRef\]](#)
26. Hubbard, C.R.; Snyder, R.L. RIR-Measurement and Use in Quantitative XRD. *Powder Diffr.* **1988**, *3*, 74–77. [\[CrossRef\]](#)
27. Kurniawan, A.; Abe, K.; Ohashi, K.; Nomura, T.; Akiyama, T. Reduction of mild-dehydrated, low-grade iron ore by ethanol. *Fuel Process. Technol.* **2018**, *178*, 156–165. [\[CrossRef\]](#)

28. Filip, J.; Karlický, F.; Marušák, Z.; Lazar, P.; Černík, M.; Otyepka, M.; Zbořil, R. Anaerobic Reaction of Nanoscale Zerovalent Iron with Water: Mechanism and Kinetics. *J. Phys. Chem. C* **2014**, *118*, 13817–13825. [[CrossRef](#)]
29. Rollason, R.J.; Plane, J.M.C. The reactions of FeO with O₃, H₂, H₂O, O₂ and CO₂. *Phys. Chem. Chem. Phys.* **2000**, *2*, 2335–2343. [[CrossRef](#)]
30. Zhao, L.-J.; Xu, X.-L.; Xu, H.-G.; Feng, G.; Zheng, W.-J. Interaction of FeO[−] with water: Anion photoelectron spectroscopy and theoretical calculations. *Phys. Chem. Chem. Phys.* **2017**, *19*, 21112–21118. [[CrossRef](#)]
31. Gilbert, F.; Refait, P.; Leveque, F.; Remazeilles, C.; Conforto, E. Synthesis of goethite from Fe(OH)₂ precipitates: Influence of Fe(II) concentration and stirring speed. *J. Phys. Chem. Solids* **2008**, *69*, 2124–2130. [[CrossRef](#)]
32. Rashid, R.Z.A.; Mohd-Salleh, H.; Ani, M.H.; Yunus, N.A.; Akiyama, T.; Purwanto, H. Reduction of low grade iron ore pellet using palm kernel shell. *Renew. Energy* **2014**, *63*, 617–623. [[CrossRef](#)]
33. Zuo, H.-B.; Hu, Z.-W.; Zhang, J.-L.; Li, J.; Liu, Z.-J. Direct reduction of iron ore by biomass char. *Int. J. Miner. Met. Mater.* **2013**, *20*, 514–521. [[CrossRef](#)]